J|A|C|S ARTICLES

Published on Web 09/23/2009

Conductance Enhancement in Nanographene−Gold Junctions by Molecular π-Stacking

Ángel J. Pérez-Jiménez* and Juan C. Sancho-García*

Departamento de Química-Física, Universidad de Alicante, E-03080 Alicante, Spain

Received May 29, 2009; E-mail: aj.perez@ua.es; jc.sancho@ua.es

Abstract: First-principles calculations on gold−pentacene−gold and several gold−circumacene−gold nanojunctions indicate that their low-bias conductance is due to the onset of a HOMO-derived resonance, thus being quite sensitive to the detailed interaction between the molecule and the gold leads. It is also found that such interaction is dominated by the electrophilic binding of Au to the (circum)acene, in agreement with previous theoretical and experimental results on pentacene. Therefore, the alignment of the HOMO resonance with the Fermi level, and thus the conductance, increases as the ionization potential and the HOMO−LUMO gap of the molecular arrangement diminish. It is shown here that both quantities are inversely proportional to the molecular length and the number of molecules present on a π stack. It is also found that the conductance depends dramatically on the amount of π overlap between the molecules in the stack, as well as on the particular disposition of the metallic tips with respect to the molecule. The conclusions reached point toward π-stacked arrangements of large circumacenes as potential candidates to build useful nanodevices for molecular electronics made out of nanographene-based materials.

1. Introduction

Graphene, a two-dimensional honeycomb lattice of sp^2-bonded carbon atoms, can be considered as the basic structural element of all other graphitic-like materials, such as graphite, carbon nanotubes, fullerenes, graphene nanoribbons, and polycyclic aromatic hydrocarbons (PAHs). Since its preparation by mechanical exfolliation, and the characterization of its extraordinary transport properties[1−8] an enormous effort has been devoted to find new synthetic routes[3,9−18] and to explore its many applications in nanoelectronics, materials science, condensed-matter physics, and low-dimensional physics.[19]

Notwithstanding this and the remarkable material properties of graphene,[20] fabricating electronic devices such as field-effect transistors (FETs) or nanoswitches out of graphene requires controlling the electrical conductivity by means of gate electrodes, which is handicapped by the absence of a bandgap in the intrinsic material.[21] In the quest to opening a significant energy gap several routes can be taken, like "rolling" graphene into carbon nanotubes,[22] forming narrow graphene stripes called

(1) Novoselov, K. S.; Geim, A. K.; Morozov, S. V.; Jiang, D.; Zhang, Y.; Dubonos, S. V.; Grigorieva, I. V.; Fisov, A. A. *Science* **2004**, *306*, 666–669.
(2) Novoselov, K. S.; Geim, A. K.; Morozov, S. V.; Jiang, D.; Katsnelson, M. I.; Grigorieva, I. V.; Dubonos, S. V.; Firsov, A. A. *Nature* **2005**, *438*, 197–200.
(3) Berger, C.; Song, Z.; Li, X.; Wu, X.; Brown, N.; Naud, C.; Mayou, D.; Li, T.; Hass, J.; Marchenkov, A. N.; Conrad, E. H.; First, P. N.; de Heer, W. A. *Science* **2006**, *312*, 1191–1196.
(4) Berger, C.; Song, Z.; Li, T.; Li, X.; Ogbazghi, A. Y.; Feng, R.; Dai, Z.; Marchenkov, A. N.; Conrad, E. H.; First, P. N.; de Heer, W. A. *J. Phys. Chem. B* **2004**, *108*, 19912–19916.
(5) Novoselov, K. S.; Jiang, D.; Booth, T. J.; Khotkevich, V. V.; Morozov, S. V.; Geim, A. K. *Proc. Natl. Acad. Sci. U.S.A.* **2005**, *102*, 10451–10453.
(6) Bunch, J. S.; Yaish, Y.; Brink, M.; Bolotin, K.; McEuen, P. L. *Nano Lett.* **2005**, *5*, 287–290.
(7) Zhang, Y.; Small, J. P.; Amori, M. E. S.; Kim, P. *Phys. Rev. Lett.* **2005**, *94*, 206803.
(8) Zhang, Y.; Tan, Y.-W.; Stormer, H. L.; Kim, P. *Nature* **2005**, *438*, 201–204.
(9) Stankovich, S.; Dikin, D. A.; Dommett, G. H. B.; Kohlhaas, K. M.; Zimney, E. J.; Stach, E. A.; Piner, R. D.; Nguyen, S. T.; Ruoff, R. S. *Nature* **2006**, *442*, 282–286.
(10) Li, D.; Müller, M. B.; Gilje, S.; Kaner, R. B.; Wallace, G. G. *Nat. Nanotechnol.* **2008**, *3*, 101–105.
(11) Wu, J.; Pisula, W.; Müllen, K. *Chem. Rev.* **2007**, *107*, 718–747.
(12) Rohrl, J.; Hundhausen, M.; Emtsev, K. V.; Seyller, T.; Graupner, R.; Ley, L. *Appl. Phys. Lett.* **2008**, *92*, 201918.
(13) Sutter, P. W.; Flege, J.-I.; Sutter, E. A. *Nat. Mater.* **2008**, *7*, 406–410.
(14) Li, X.; Wang, X.; Zhang, L.; Lee, S.; Dai, H. *Science* **2008**, *319*, 1229–1232.
(15) Wang, X.; Ouyang, Y.; Li, X.; Wang, H.; Guo, J.; Dai, H. *Phys. Rev. Lett.* **2008**, *100*, 206803.
(16) Dato, A.; Radmilovic, V.; Lee, Z.; Phillips, J.; Frenklach, M. *Nano Lett.* **2008**, *8*, 2012–2016.
(17) Li, X.; Zhang, G.; Bai, X.; Sun, X.; Wang, X.; Wang, E.; Dai, H. *Nat. Nanotechnol.* **2008**, *3*, 538–542.
(18) Tang, Y. B.; Lee, C. S.; Chen, Z. H.; Yuan, G. D.; Kang, Z. H.; Luo, L. B.; Song, H. S.; Liu, Y.; He, Z. B.; Zhang, W. J.; Bello, I.; Lee, S. T. *Nano Lett.* **2009**, *9*, 1374–1377.
(19) Geim, A. K.; Novoselov, K. S. *Nat. Mater.* **2007**, *6*, 183–191.
(20) Lee, C.; Wei, X.; Hone, J. *Science* **2008**, *321*, 385–388.
(21) Oostinga, J. B.; Heersche, H. B.; X. Liu, A. F. M.; Vandersypen, L. M. K. *Nat. Mater.* **2008**, *7*, 151–157.
(22) Ijima, S. *Nature* **1991**, *354*, 56–58.
(23) Han, M.; Oezylmaz, B.; Zhang, Y.; Kim, P. *Phys. Rev. Lett.* **2007**, *98*, 206805.
(24) Chen, Z.; Lin, Y.-M.; Rooks, M. J.; Avouris, P. *Physica E* **2007**, *40*, 228–232.
(25) Schniepp, H. C.; Li, J.-L.; McAllister, M. J.; Sai, H.; Herrera-Alonso, M.; Adamson, D. H.; Prud'homme, R. K.; Car, R.; Saville, D. A.; Aksay, I. A. *J. Phys. Chem. B* **2006**, *110*, 8535–8539.
(26) Rollings, E.; Gweon, G.-H.; Zhou, S.; Mun, B.; McChesney, J.; Hussain, B.; Fedorov, A.; First, P.; de Heer, W.; Lanzara, A. *J. Phys. Chem. Solids* **2006**, *67*, 2172–2177.

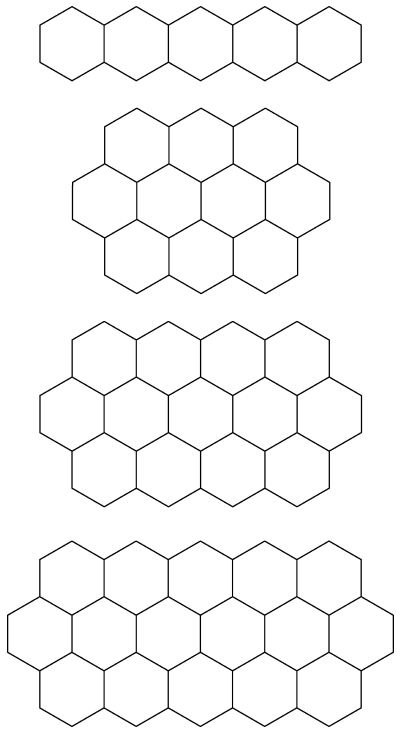

Figure 1. Carbon backbone of the molecules considered in the paper. From top to bottom: pentacene (P), circumnaphthalene (CN), circumanthracene (CA) and circumtetracene (CT).

graphene nanoribbons (GNRs),[14,23−28] or stacking graphene layers as in bilayer graphene (BG).[21,29]

Both GNRs and BG have recently demonstrated to be remarkably good candidate materials to build nanoelectronic devices because of their band gap engineering capabilities. The peculiar electronic structure of BG[29−31] allows the external control of the bandgap width,[21,29,32−34] thus being the only known semiconductor with a tunable energy gap.[32] On the other hand, infinitely long GNRs represent versatile materials because of their tunable magnetic and electronic properties.[3,35−49]

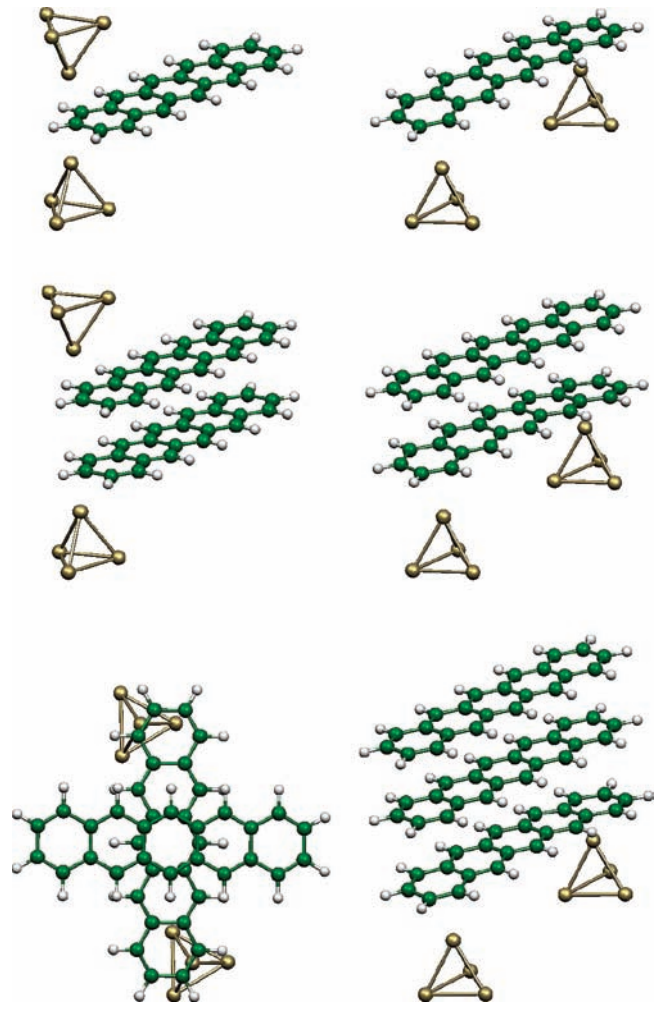

Figure 2. Geometries of gold−P−gold nanobridges. From left to right and from top to bottom: *os* × 1, *ss* × 1, *os* × 2, *ss* × 2, *ss* × 2-TS, and *ss* × 3.

"Zero-dimensional", finite GNRs develop HOMO−LUMO gaps that can also be modified in a number of ways, with potential applications as half metals[44,48,50,51] or as building blocks of FETs.[14,15,18,41] Additionally, the magnetic properties of such systems have been subject of recent scrutiny.[49,52−56] The calculations performed on some PAHs, like oligoacenes, periacenes, and circumacenes,[55,57−59] indicate that these zero-

(27) Yang, X.; Dou, X.; Rouhanipour, A.; Zhi, L.; Rader, H. J.; Mullen, K. *J. Am. Chem. Soc.* **2008**, *130*, 4216–4217.
(28) Kosynkin, D. V.; Higginbotham, A. L.; Sinitskii, A.; Lomeda, J. R.; Dimiev, A. *Nature* **2009**, *458*, 872–876.
(29) Ohta, T.; Bostwick, A.; Seyller, T.; Horn, K.; Rotenberg, E. *Science* **2006**, *313*, 951–954.
(30) McCann, E.; Fal'ko, V. I. *Phys. Rev. Lett.* **2006**, *96*, 086805.
(31) Nilsson, J.; Neto, A. H. C.; Guinea, F.; Peres, N. M. R. *Phys. Rev. Lett.* **2006**, *97*, 266801.
(32) Castro, E. V.; Novoselov, K. S.; Morozov, S. V.; Peres, N. M. R.; Lopes dos Santos, J. M. B.; Nilsson, J.; Guinea, F.; Geim, A. K.; Castro Neto, A. H. *Phys. Rev. Lett.* **2007**, *99*, 216802.
(33) Ouyang, Y.; Campbell, P.; Guo, J. *Appl. Phys. Lett.* **2008**, *92*, 063120.
(34) Fiori, G.; Iannaccone, G. *IEEE Electron. Device Lett.* **2009**, *30*, 261–264.
(35) Nakada, K.; Fujita, M.; Dresselhaus, G.; Dresselhaus, M. S. *Phys. Rev. B* **1996**, *54*, 17954–17961.
(36) Wakabayashi, K.; Fujita, M.; Ajiki, H.; Sigrist, M. *Phys. Rev. B* **1999**, *59*, 8271–8282.
(37) Kusakabe, K.; Maruyama, M. *Phys. Rev. B* **2003**, *67*, 092406.
(38) Hod, O.; Barone, V.; Peralta, J. E.; Scuseria, G. E. *Nano Lett.* **2007**, *7*, 2295–2299.
(39) Naeemi, A.; Meindl, J. D. *IEEE Electron. Device Lett.* **2007**, *28*, 428–431.
(40) Sols, F.; Guinea, F.; Neto, A. H. C. *Phys. Rev. Lett.* **2007**, *99*, 166803.
(41) Liang, G.; Neophytou, N.; Lundstrom, M. S.1; Nikonov, D. E. *Nano Lett.* **2008**, *8*, 1819–1824.
(42) Kudin, K. N. *ACS Nano* **2008**, *2*, 516–522.
(43) Hod, O.; Peralta, J. E.; Scuseria, G. E. *Phys. Rev. B* **2007**, *76*, 233401.
(44) Kan, E.; Li, Z.; Yang, J.; Hou, J. G. *J. Am. Chem. Soc.* **2008**, *130*, 4224–4225.
(45) Rozhkov, A. V.; Savel'ev, S.; Nori, F. *Phys. Rev. B* **2009**, *79*, 125420.
(46) Hosoya, H.; Kumazaki, H.; Chida, K.; Ohuchi, M.; Gao, Y. D. *Pure Appl. Chem.* **1990**, *62*, 445–450.
(47) Ezawa, M. *Phys. Rev. B* **2006**, *73*, 045432.
(48) Barone, V.; Hod, O.; Scuseria, G. E. *Nano Lett.* **2006**, *6*, 2748–2754.
(49) Shemella, P.; Zhang, Y.; Mailman, M.; Ajayan, P. M.; Nayak, S. K. *Appl. Phys. Lett.* **2007**, *91*, 042101.
(50) Son, Y.-W.; Cohen, M. L.; Louie, S. G. *Nature* **2006**, *444*, 347–349.
(51) Rudberg, E.; Salek, P.; Luo, Y. *Nano Lett.* **2007**, *7*, 2211–2213.
(52) Yamashiro, A.; Shimoi, Y.; Harigaya, K.; Wakabayashi, K. *Phys. Rev. B* **2003**, *68*, 193410.
(53) Fernández-Rossier, J.; Palacios, J. J. *Phys. Rev. Lett.* **2007**, *99*, 177204.
(54) Ezawa, M. *Phys. Rev. B* **2007**, *76*, 245415.
(55) Hod, O.; Barone, V.; Scuseria, G. E. *Phys. Rev. B* **2008**, *77*, 035411.
(56) Munoz-Rojas, F.; Fernández-Rossier, J.; Palacios, J. J. *Phys. Rev. Lett.* **2009**, *102*, 136810.
(57) Jiang, D.; Sumpter, B. G.; Dai, S. *J. Chem. Phys.* **2007**, *127*, 124703.
(58) Jiang, D.; Dai, S. *J. Phys. Chem. A* **2008**, *112*, 332–335.
(59) Jiang, D.; Dai, S. *Chem. Phys. Lett.* **2008**, *466*, 72–75.

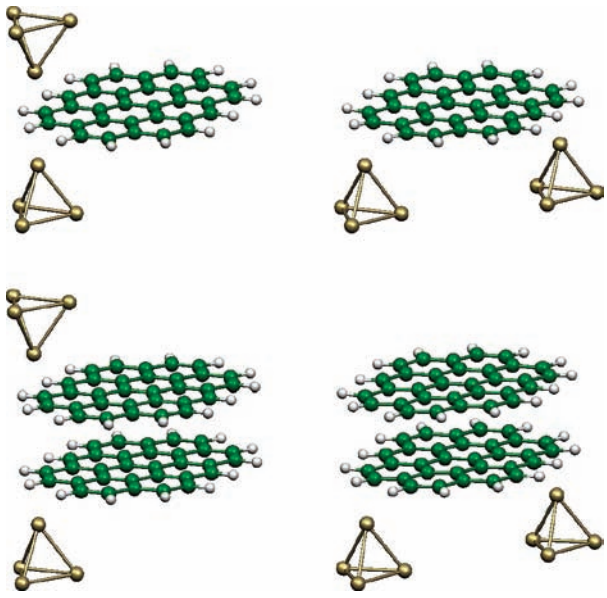

Figure 3. Geometries of gold−CN−gold nanobridges. From left to right and from top to bottom: *os* × 1, *ss* × 1, *os* × 2, *ss* × 2. The structures of similar gold−CA−gold and gold−CT−gold nanobridges are not included because, apart from the increased size of the molecule, they are completely analogous to the gold−CN−gold ones shown here.

dimensional GNRs, which can be considered as "nanographenes",[57] present a spin-polarized ground state beyond a certain (usually small) length.

Some of these molecules, specially pentacene and pentacene derivatives, have also been used as key components in nanoelectronics.[60−68] As is also the case for other molecules and graphene-based materials, their charge transport properties are critically dependent on the alignment between the HOMO or LUMO levels of the molecules with the metal states and are thus quite sensitive to both the HOMO−LUMO gap of the original molecule and to the molecule−metal interaction.[60−65,67−70] In previous works,[71,72] we have highlighted the relationship between structural and transport properties of pentacene (P) and small circumacenes such as circumnaphthalene (CN) and circumanthracene (CA) (see Figure 1), which in the following will be collectively termed (circum)acenes. It was concluded that charge transfer rates of circumacenes are systematically larger than those of oligoacenes of the same size, basically because of a decrease in the electron−phonon coupling caused by the more rigid carbon backbone of the former as compared to the latter.[71] We have also found that the relative trends found for the charge transfer properties of P, CN, and CA in the hopping regime are also found in the coherent charge transport regime typical of gold-molecule-gold nanobridges. Although a quantitative justification of this finding requires knowledge of the metal-contact geometry of the nanobridge, a qualitative explanation could also be established from the interrelationship between structural parameters and the HOMO−LUMO gap of the molecules.[72]

In this work, we continue the study recently started with the main objective of exploring several possibilities to modulate the electron transport properties of graphene-based nanodevices, by considering gap modifications induced by changing the molecular length and/or their π-stacking. In addition to P, CN, and CA, we will also include circumtetracene (CT) in our study to have a much firmer basis to discuss the influence of the molecular length. We focus on these four nonmagnetic[58,59] molecules for three main reasons. (i) Their molecular stability: P, CN, and CA have already been synthesized while CT is predicted to be a stable molecule;[59,73] (ii) their versatility, thanks to the large variation of the ionization potential, *I*, and HOMO−LUMO gap of (circum)acenes with their size;[74] (iii) the strength of the direct gold-acene interaction, which is supported by recent experimental and numerical evidence.[60,72,75−78]

Our results suggest that gold−molecule−gold nanojunctions built from long circumacenes, such as CT, are good candidates to build FETs with high conductance "on" states and on−off conductance ratios around 1×10^3. It is also found that the possible molecular π-stacking of (circum)acene molecules during the fabrication process of the nanobridge may alter the conductance depending on the cofacial or noncofacial character of the stack. The above facts and their rationalization will be addressed in section 3 of the paper while first, in section 2, a description of the method used to calculate the conductance will be given. Finally, a summary of the main conclusions will be outlined in section 4.

2. Computational Methods

2.1. Calculating the Conductance of Molecular Nanobridges. Our approach to compute the conductance, $\mathscr{G}$, of a nanodevice is based on four major premises that we outline next:

(1) Elastic coherent transport. We will assume that the electron transport through gold−molecule−gold nanobridges occurs without significant nuclear reorganization of the system, which is usually an excellent approximation because the transferred electron does not stay localized on the molecular species.[69] Disregarding thermal interactions also during the transmission process the latter can be considered as resulting from the scattering of electrons through a barrier characterized by the transmission function *T* (elastic coherent transport). In the low-temperature limit, the conductance is related to *T* through the well-known Landauer's formula

$$\mathscr{G} = \frac{e^2}{\pi\hbar} T(E_F) = G_0 T(E_F) \qquad (1)$$

where E_F is the Fermi level of the system and $G_0 \equiv e^2/\pi\hbar$.

(2) Formal division of the nanodevice. By considering that the system is composed of a finite scattering section enclosing the

(60) Ferretti, A.; Baldacchini, C.; Calzolari, A.; Di Felice, R.; Ruini, A.; Molinari, E.; Betti, M. G. *Phys. Rev. Lett.* **2007**, *99*, 046802.
(61) Ihm, K.; Chung, S.; Kang, T.-H.; Cheong, S.-W. *Appl. Phys. Lett.* **2008**, *93*, 141906.
(62) Sawabe, T.; Okamura, K.; Sueyoshi, T.; Miyamoto, T.; Kudo, K.; Ueno, N.; Nakamura, M. *Appl. Phys. A: Mater. Sci. Process.* **2009**, *95*, 225–232.
(63) Tada, T.; ad M. Kondo, D. N.; Hamayama, S.; Yoshizawa, K. *J. Am. Chem. Soc.* **2004**, *126*, 14182–14189.
(64) Kim, B.; Beebe, J. M.; Jun, Y.; Zhu, X.-Y.; Frisbie, C. D. *J. Am. Chem. Soc.* **2006**, *128*, 4970–4971.
(65) Quinn, J. R.; Foss, F. W., Jr.; Venkataraman, L.; Hybertsen, M. S.; Breslow, R. *J. Am. Chem. Soc.* **2007**, *129*, 6714–6715.
(66) Zhou, Y. X.; Jiang, F.; Chen, H.; Note, R.; Mizuseki, H.; Kawazoe, Y. *Phys. Rev. B* **2007**, *75*, 245407.
(67) Pan, Z.; Li, Q.-X.; Shi, Q.-W.; Wang, X.-P. *Chin. J. Chem. Phys.* **2008**, *22*, 7–12.
(68) Chen, F.; Tao, N. J. *Acc. Chem. Res.* **2009**, *42*, 429–438.
(69) Nitzan, A. *Annu. Rev. Phys. Chem.* **2001**, *52*, 681–750.
(70) Lindsay, S. M.; Ratner, M. A. *Adv. Mater.* **2007**, *19*, 23–31.
(71) Sancho-García, J. C.; Pérez-Jiménez, A. J. *Phys. Chem. Chem. Phys.* **2009**, *11*, 2741–2746.
(72) Pérez-Jiménez, A. J.; Sancho-García, J. C. *Nanotechnology*, submitted.
(73) Broene, R. D.; Diederich, F. *Tetrahedron Lett.* **1991**, *32*, 5227–5230.
(74) Biermann, D.; Schmidt, W. *J. Am. Chem. Soc.* **1980**, *102*, 3163–3173.
(75) Repp, J.; Meyer, G.; Paavilainen, S.; Olsson, F. E.; Persson, M. *Science* **2006**, *312*, 1196–1199.

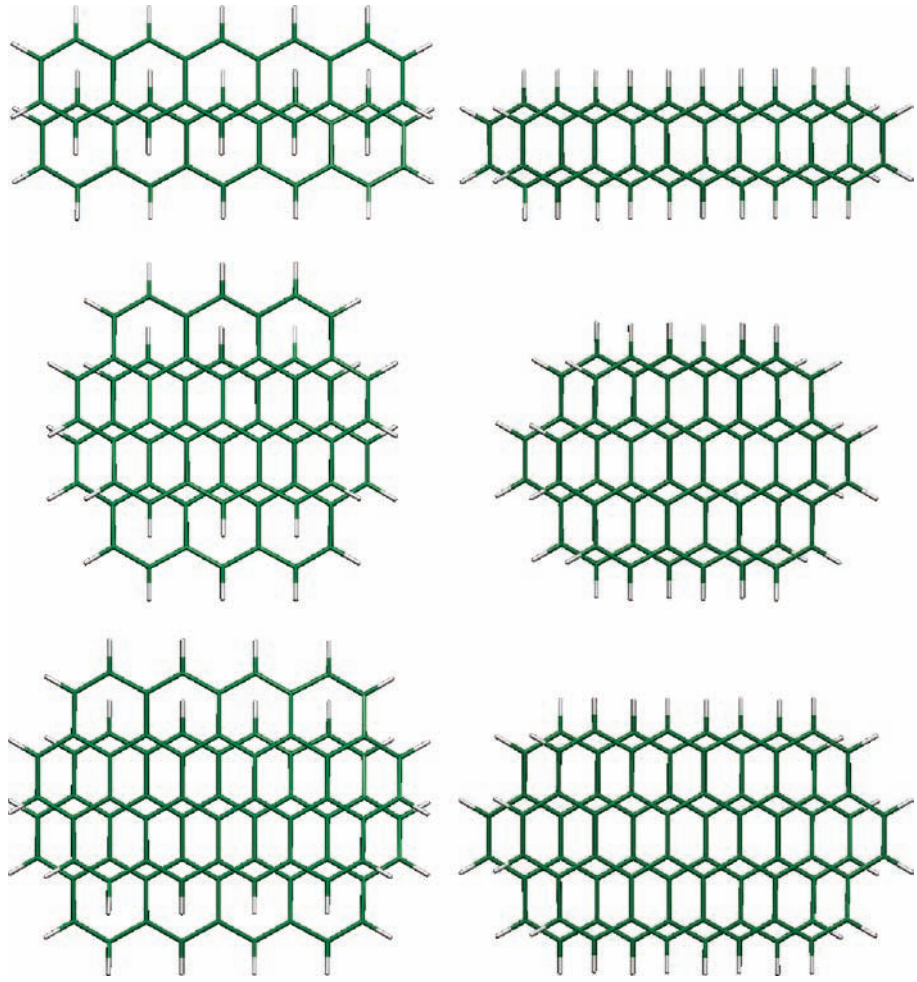

Figure 4. Top view of geometries corresponding to parallel-displaced gold−(circum)acene−gold *ss* nanobridges (the metallic tips, whose position is the same than for cofacially π-stacked *ss* nanobridges, have been removed for clarity). From top to bottom: P, CN, CA. Left: parallel-displaced dimeric structures along the short axis (*ss* × 2-PD1). Right: parallel-displaced dimeric structures along the long axis (*ss* × 2-PD2).

molecule and a small portion of the metallic leads (hereafter termed "cluster") and two semi-infinite leads (electron reservoirs) attached to it, $T(E)$ can be conveniently computed from

$$T(E) = \mathrm{Tr}[\mathbf{\Gamma}_L(E)\mathbf{G}_C^r(E)\mathbf{\Gamma}_R(E)\mathbf{G}_C^a(E)] = \mathrm{Tr}[\mathbf{t}^\dagger(E)\mathbf{t}(E)] \quad (2)$$

$$\mathbf{t}(E) \equiv \mathbf{\Gamma}_R^{1/2}(E)\mathbf{G}_C^a(E)\mathbf{\Gamma}_L^{1/2}(E) \quad (3)$$

reflecting that T and the corresponding scattering matrix, **t**, depend on how the electrons propagate through the cluster (C), as determined by its retarded and advanced Green's matrices $\mathbf{G}_C^{r,a}$ and also on the interaction between the cluster with the left (L) and right (R) leads as determined by the corresponding coupling matrices $\Gamma_{L,R}(E)$.

The Green's function formalism used in eqs 2 and 3 allows us to take an important conceptual step by replacing the infinite open system composed by two semi-infinite leads connected through a molecular conductor (cluster) by an equivalent but finite one where the effect of the leads on the conductor is incorporated in $\mathbf{G}_C$ by means of the so-called self-energy matrices $\sum_{L,R}^r(E)$:

$$\mathbf{G}_C^r(E) = [(E + i\eta)\mathbf{S}_C - \mathbf{H}_C - \mathbf{\Sigma}_L^r(E) - \mathbf{\Sigma}_R^r(E)^{-1} \quad (4)$$

where $\mathbf{S}_C$ and $\mathbf{H}_C$ represent overlap and Hamiltonian matrices evaluated over an appropriate atomic basis set defined in the cluster region. The self-energy matrices act as a kind of "effective" field that modifies the Green's matrix of the isolated cluster, $\mathbf{G}_{C,isol}^r(E) = [(E + i\eta)\mathbf{S}_C - \mathbf{H}_C]^{-1}$, altering the corresponding eigenstates of the isolated system in two ways: the real part of shifts their eigenenergies, whereas the imaginary part

$$Im\ \mathbf{\Sigma}_{L,R}^r(E) = -\frac{1}{2}\mathbf{\Gamma}_{L,R}(E) \quad (5)$$

gives them finite lifetimes, allowing electrons to escape/enter from/to them.

(3) Bethe lattice model for the metallic leads. Application of eqs 2 and 4 above requires the evaluation of the self-energies. Here we use, the approach followed by Palacios et al.[79−82] and obtain them by modeling the leads by a tight-binding Bethe lattice model.

(76) Yang, G.; Fang, L.; Tan, K.; Shi, S.; Su, Z.; Wang, R. *Organometallics* **2007**, *26*, 2082–2087.
(77) Sun, S.-L.; Qin, C.-S.; Qiu, Y.-Q.; Yang, G.-C.; Su, Z.-M. *J. Organomet. Chem.* **2009**, *694*, 1266–1272.
(78) Korventausta, A.; Paavilainen, S.; Niemi, E.; Nieminen, J. A. *Surf. Sci.* **2009**, *603*, 437–444.
(79) Palacios, J. J.; Pérez-Jiménez, A. J.; Louis, E.; Vergés, J. A. *Phys. Rev. B* **2001**, *64*, 115411.
(80) Palacios, J. J.; Pérez-Jiménez, A. J.; Louis, E.; SanFabián, E.; Vergés, J. A. *Phys. Rev. B* **2002**, *66*, 035322.
(81) Louis, E.; Vergés, J. A.; Palacios, J. J.; Pérez-Jiménez, A. J.; SanFabián, E. *Phys. Rev. B* **2003**, *67*, 155321.
(82) Palacios, J. J.; Pérez-Jiménez, A. J.; Louis, E.; SanFabián, E.; Vergés, J. A.; García, Y. Molecular electronics with Gaussian98/03. In *Computational Chemistry: Reviews of Current Trends*; Leszczynski, J., Ed.; World Scientific: Singapore, 2005; Vol. 9.

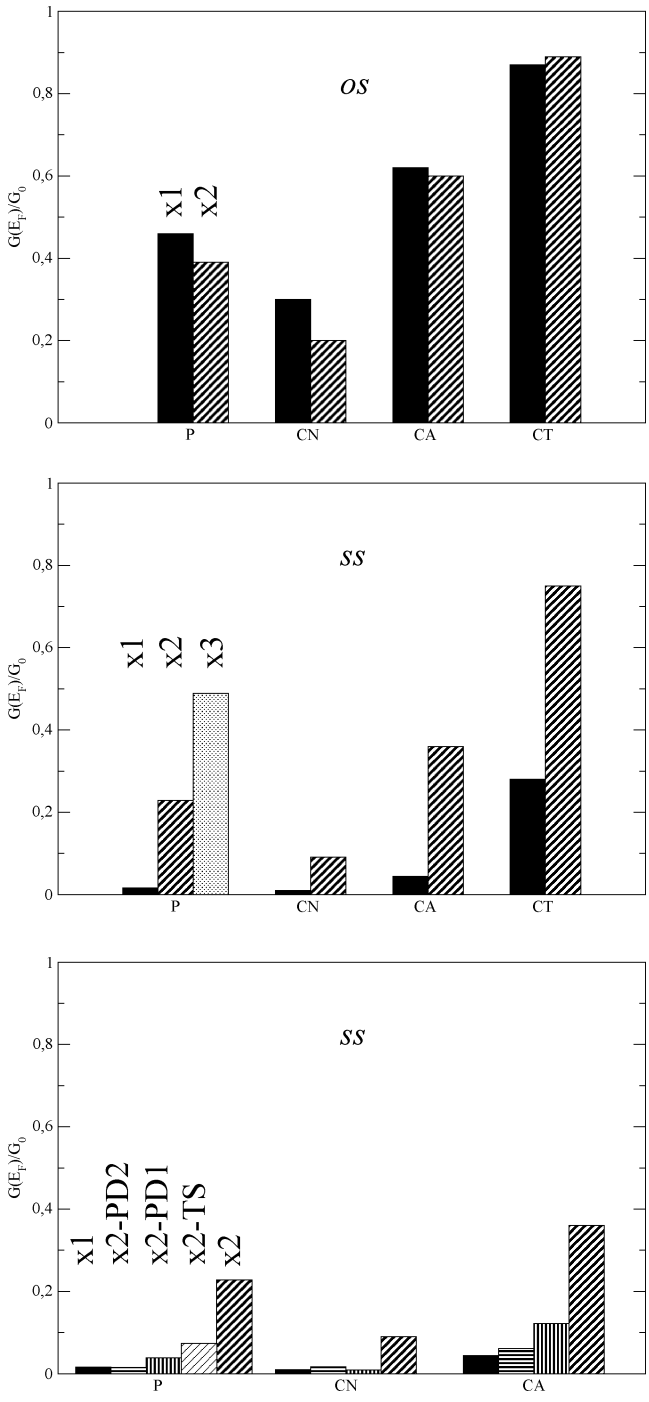

Figure 5. Conductance at zero bias of gold−molecule−gold nanobridges for pentacene (P), circumnaphthalene (CN), circumanthracene (CA), and circumtetracene (CT). Top: cofacial *os* nanojunctions. Middle: cofacial *ss* nanojunctions. Bottom: noncofacial *ss* nanojunctions. Black: one molecule (× 1). Dark diagonal stripes: two cofacial molecules (× 2). Dark horizontal stripes: two parallel-displaced molecules along the long axis (× 2-PD2). Dark vertical stripes: two parallel-displaced molecules along the short axis (× 2-PD1). Light diagonal stripes: two molecules rotated 90° (× 2-TS). Dotted: three cofacial molecules (× 3).

(4) Determination of the Fermi energy. The positioning of the Fermi energy is key to obtain a correct value for the conductance. We determine it in a self-consistent fashion by guaranteeing charge neutrality in the cluster region once attached to the semi-infinite leads, thus providing the proper alignment between the molecular resonances and the Fermi energy.[82]

The values of T and $\mathscr{G}$ have been calculated with the implementation of the procedure outlined above made in the ALACANT[83] program, interfaced with the Gaussian03 package.[79−82,84] The Hamiltonian and overlap matrices of the cluster region are evaluated within the Kohn−Sham density functional theory (KSDFT) using the B3LYP exchange-correlation functional, together with the 6-31G* basis set for C and H, and the Christiansen and co-workers pseudopotential and basis set for Au.[85] We have selected the B3LYP functional because the correctness of the transmission calculations depend on accurate estimates of the molecule−metal nanocontact geometry and the HOMO−LUMO gap for the transmission calculations, and the B3LYP functional is able to achieve both.[76,77,86−88]

2.2. Cluster Geometries. The geometries of the clusters used in the conductance calculations with a single molecule attached to the metallic leads correspond to KSDFT-B3LYP constrained optimizations performed in ref 72 with the same basis set and pseudopotentials used in the conductance calculations. They are shown in Figures 2 and 3. They can be grouped in two different sets according to the way that the metallic tips adopt with respect to the molecule: either at "opposite sides" (*os*) or at the "same side" (*ss*) of the molecular plane. They are labeled "*os* × *m*" and "*ss* × *m*", respectively, with *m* being the number of molecules present in the nanojunction (see below). By using such different binding geometries, we try to take into account the diversity of contact geometries expected in mechanically formed molecular junctions.[89−91] It was found in ref 72 that both types of structures are rather stable thanks to the presence of unsaturated gold atoms in the metal contacts, in nice agreement with recent experiments[75] and theoretical calculations[76,77] where a single Au atom binds to a pentacene molecule. The distance between the gold atom at the tip apex and the nearest carbon atom is about 2.4 Å, in good agreement with the values calculated in refs 76 and 77.

The gold tips are modeled by two-slab structures of 4 gold atoms each along the [111] direction of an fcc crystal with a lattice constant of 4.0786 Å. Enlarging the metal portion of the clusters to 10 gold atoms per tip provides the same relative trends obtained with 4-atom tips[72] and will thus not be considered here.

We have considered mainly two kinds of cluster geometries involving π-stacked molecules: perfectly cofacial and parallel-displaced configurations. The latter are usually found as the lowest energy structures for aggregates of small PAHs, whereas the former represent low-lying high-symmetry configurations.[92,93] Our reasons to focus on these two types of stacked clusters among the wide range of geometries that have been proposed are basically the same that guided our choice of molecule-tip arrangements: they represent two extreme cases for the quite uncontrolled molecular π-stacking observed in the fabrication of graphene-based nanojunctions.[14,28] The perfectly cofacial dimers, which are also shown in Figures 2 and 3, are built from their single-molecule counterparts by placing the additional molecules at a distance of 3.5 Å from each other and translating correspondingly the gold tips for the *os*-like structures. The interplanar distance has been chosen as an inter-

(83) Palacios, J. J.; Pérez-Jiménez, A. J.; Jacob, D.; Louis, E.; San-Fabián, E.; Vergés, J. A. http://www.guirisystems.com/alacant.
(84) Frisch, M. J.; et al. *GAUSSIAN03, Revision B.01*; Gaussian, Inc.: Pittsburgh, PA, 2003.
(85) Roos, R. B.; Powers, J. M.; Atashroo, T.; Ermler, W. C.; LaJohn, L. A.; Christiansen, P. A. *J. Chem. Phys.* **1990**, *93*, 6654–6670.
(86) Schultz, N. E.; Zhao, Y.; Truhlar, D. G. *J. Phys. Chem. A* **2005**, *109*, 11127–11143.
(87) Kümmel, S.; Kronik, L. *Rev. Mod. Phys.* **2008**, *80*, 3–60.
(88) Kadantsev, E. S.; Stott, M. J.; Rubio, A. *J. Chem. Phys.* **2006**, *124*, 134901.
(89) Nazin, G. V.; Qiu, X. H.; Ho, W. *Science* **2003**, *302*, 77–81.
(90) Cheng, F.; Hihath, J.; Huang, Z.; Li, X.; Tao, N. J. *Annu. Rev. Phys. Chem.* **2007**, *58*, 535–564.
(91) Akkerman, H. B.; de Boer, B. *J. Phys.: Condens. Matter.* **2008**, *20*, 013001.
(92) Rapacioli, M.; Calvo, F.; Spiegelman, F.; Joblin, C.; Wales, D. J. *J. Phys. Chem. A* **2005**, *109*, 2487–2497.
(93) Zhao, Y.; Truhlar, D. G. *J. Phys. Chem. C* **2008**, *112*, 4061–4067.

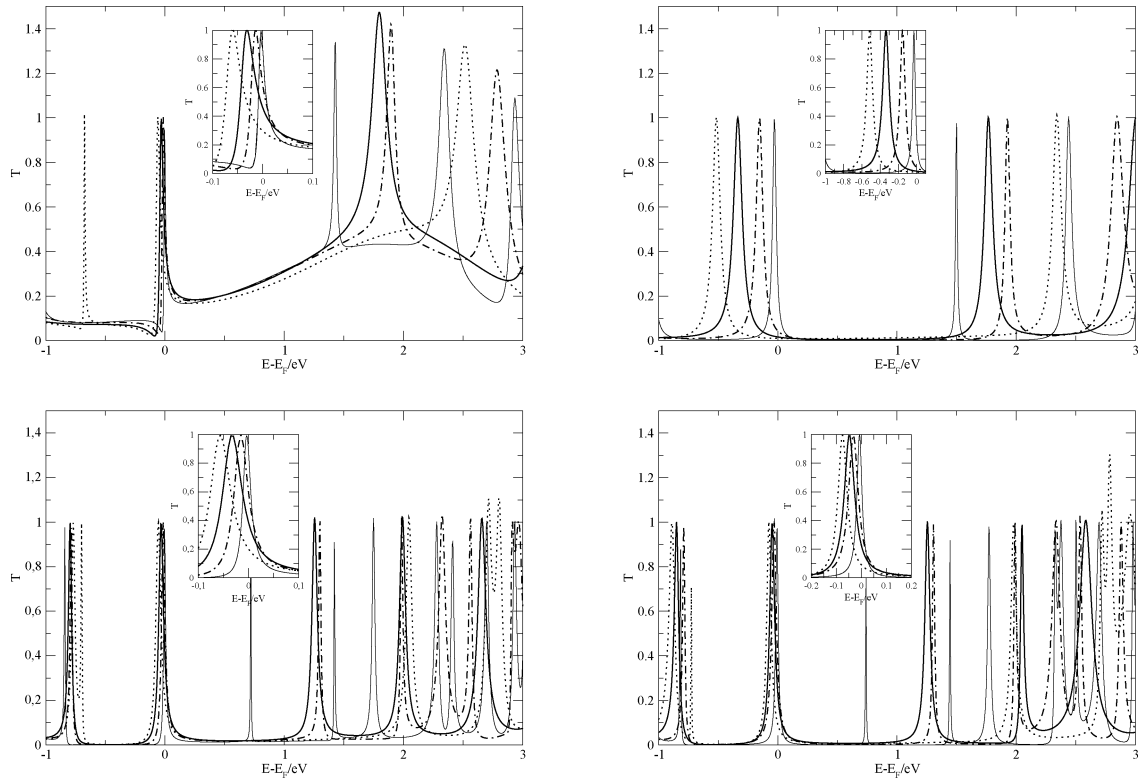

Figure 6. Transmission profiles of single-molecule and cofacially- π-stacked gold−(circum)acene−gold nanobridges. Dark solid, pentacene; dotted, circumnaphthalene; dotted-dashed, circumanthracene; light solid, circumtetracene. Top left: *os* × 1. Top right: *ss* × 1. Bottom left: *os* × 2. Bottom right: *ss* × 2.

mediate value between that of graphite, 3.35 Å,[94] and the value ∼3.6−3.7 Å estimated from recent geometry optimizations on cofacial coronene dimers.[93] On the other hand, and inspired by such recent work on coronene dimers we consider noncofacial dimeric structures where one molecule sits above the other at an interplane distance of 3.33 Å and is parallel-displaced with respect to it by 1.75 Å (1.45 Å) along the direction of its short (long) axis, see Figure 4, hereafter labeled × 2-PD1 (× 2-PD2). The symmetry loss of the displaced geometries increases the computational load, and for that reason we only show transport calculations for the smallest three molecules (P, CN, and CA) and only for the *ss*-like metal-molecule disposition. Notwithstanding this, the transport calculations clearly indicate that the changes in $\mathscr{G}$ as a consequence of the displacement are due to the same acute lowering of the overlap for the three molecules considered, and this is expected to occur for the remaining one: circumtetracene. The role of the overlap is also confirmed by studying a "twisted sandwich" (TS) dimeric structure[93] for pentacene, labeled × 2-TS, where one molecule is rotated 90° with respect to the other; see Figure 3. We have not taken into account "T-shaped" dimeric structures, where the planes of the two molecules are perpendicular to each other, because they are expected to have much higher energies.[93]

Before closing this section, we want to point out that the approach taken here to build the π-stacked structures by placing the optimized monomer geometries at a fixed position is quite common in computational studies, given the difficulties that many exchange-correlation functionals face to appropriately account for the dispersion forces entering the problem.[93,94] Although it is well-known that B3LYP is one of such functionals, we want to stress that for the transport calculations, it is of utmost importance to correctly estimate the molecular gap and the alignment between the Fermi level and the molecular levels, two tasks for which the B3LYP functional seems to be a reasonable candidate.[76,77,86−88] Furthermore, despite the fact that B3LYP provides wrong values for the binding energies of PAHs dimers, we have checked that, once empirically corrected post-SCF (i.e., without altering the original B3LYP electronic structure) with damped atom-pairwise-$C_6 \cdot R^{-6}$ potentials[95] (B3LYP-D) it yields the correct relative ordering for coronene dimers with respect to the most stable PD1 configuration: PD2 (+0.1 kcal/mol) < TS (+1.2 kcal/mol) < cofacial (+7.2 kcal/mol); as compared with that corresponding to the dispersion-validated M06−2X functional:[96] PD2 (+0.8 kcal/mol) < TS (+0.9 kcal/mol) < cofacial (+9.4 kcal/mol).[93] In light of the former evidence, we believe that the B3LYP exchange-correlation functional is indeed a sound choice to study the kind of properties and systems we are interested in with this work.

3. Results and Discussion

Figure 5 plots the conductance at the Fermi energy calculated for the systems described in the previous sections, from which the following facts can be highlighted.

1. The conductance always increases with the molecular length in the order CN < P < CA < CT.

2. The conductance of *os* nanobridges is systematically larger than that corresponding to *ss* ones, especially for single molecule systems.

3. $\mathscr{G}(E_F)$ for *os* nanobridges with two cofacially π-stacked molecules is on the same order of magnitude as that obtained with a single molecule. However, *ss* nanobridges with two cofacially π-stacked molecules yield values of $\mathscr{G}(E_F)$ much larger than their single-molecule counterparts.

(94) Grimme, S.; Mück-Lichtenfeld, C.; Antony, J. *J. Phys. Chem. C* **2007**, *111*, 11199–11207.
(95) Grimme, S. *J. Comput. Chem.* **2006**, *27*, 1787–1799.
(96) Zhao, Y.; Truhlar, D. G. *Theor. Chem. Acc.* **2007**, *120*, 215–241.

Table 1. HOMO and LUMO Energies (reversed sign), and Corresponding Gaps of Isolated P, CN, CA, and CT Molecules and π-Stacked Structures, Together with the Energy Gaps (Δ_g) and Electron Charge Transfer from a Mulliken Population Analysis (q) of the Corresponding Gold−Molecule−Gold Nanobridges Built from Them

system	$-\varepsilon_H$ (eV)	$-\varepsilon_L$ (eV)	E_g (eV)	Δ_g (eV)	q (e)
		P			
isolated					
× 1	4.60	2.39	2.21		
× 2-TS	4.49	2.37	2.12		
× 2-PD1	4.43	2.53	1.90		
× 2-PD2	4.38	2.36	2.02		
× 2	4.14	2.53	1.61		
× 3	3.84	2.56	1.28		
os nanobridges					
× 1				1.83	0.80
× 2				1.29	0.99
ss nanobridges					
× 1				2.11	0.74
× 2-TS				1.63	0.83
× 2-PD1				1.56	0.83
× 2-PD2				1.71	0.87
× 2				1.36	0.91
× 3				1.08	1.06
		CN			
isolated					
× 1	4.93	2.01	2.92		
× 2-PD1	4.64	2.03	2.61		
× 2-PD2	4.62	1.98	2.64		
× 2	4.38	2.18	2.20		
os nanobridges					
× 1				2.58	0.69
× 2				2.10	0.90
ss nanobridges					
× 1				2.85	0.68
× 2-PD1				2.32	0.82
× 2-PD2				2.34	0.83
× 2				2.06	0.92
		CA			
isolated					
× 1	4.60	2.45	2.15		
× 2-PD1	4.34	2.49	1.85		
× 2-PD2	4.33	2.42	1.91		
× 2	4.05	2.59	1.46		
os nanobridges					
× 1				1.91	0.86
× 2				1.32	1.10
ss nanobridges					
× 1				2.08	0.83
× 2-PD1				1.70	0.97
× 2-PD2				1.78	0.97
× 2				1.34	1.08
		CT			
isolated					
× 1	4.35	2.75	1.60		
× 2-PD1	4.16	2.80	1.36		
× 2-PD2	4.14	2.72	1.42		
× 2	3.81	2.88	0.93		
os nanobridges					
× 1				1.44	1.01
× 2				0.73	1.02
ss nanobridges					
× 1				1.53	0.91
× 2				0.75	1.32

4. The conductance of *ss* nanobridges increases with the number of cofacially π-stacked molecules.

5. Non cofacial π-stacked *ss* nanobridges give values of $\mathscr{G}(E_F)$ much lower than the corresponding cofacial ones.

Points 1−5 above will be explained next by recognizing that the conductance is governed by the width and the alignment of a HOMO-derived resonance with the Fermi energy in the corresponding transmission profiles. It will be shown that the alignment mostly depends on the ionization potential and HOMO−LUMO gap of the molecular arrangement, which can be varied by using (circum)acenes with different sizes and/or π stacking them, whereas the resonance width decreases dramatically for noncofacial structures because of the corresponding overlap loss.

3.1. Single-Molecule Nanojunctions. Figure 6 plots transmission curves around the Fermi level for single-molecule gold−(circum)acene−gold nanobridges corresponding to *os* and *ss* structures. The peak placed near the Fermi level corresponds to a HOMO-derived resonance of the molecule,[72] and its alignment with E_F governs the actual conductance of the nanodevice. This situation is analogous to that experimentally found for some gold−diaminoacene nanobridges[65] and theoretically predicted for gold−oligoacene dithiolate nanodevices.[67] When this occurs, the length−conductance relationship deviates from Magoga's law, and an increase in the conductance is expected as the length of the (circum)acene molecule increases because both the ionization potential I, which in the Kohn−Sham formalism corresponds to minus the HOMO energy (ε_H),[97,98] and the HOMO−LUMO gap ($E_g \equiv \varepsilon_L - \varepsilon_H$, where ε_L represents the LUMO energy) diminish,[74] thus favoring the above-mentioned alignment between the HOMO-derived resonance and the Fermi level. Such behavior is consistent with both the transmission profiles shown in Figure 6, where the HOMO-E_F alignment and the conductance increases in the order CN < *P* < CA < CT, and the values of $-\varepsilon_H$ and gaps listed in Table 1, which decrease in the same order. Another key parameter that affects the conductance through the HOMO-E_F alignment is the amount of charge transferred between the molecular arrangement and the metallic tips. According to recent experimental and theoretical works the bonding of a gold atom to a pentacene molecule[75−77] is quite strong and electrophilic, with a small net electron transfer from the molecule to the gold atom caused by the larger electronegativity of the latter as compared to that of the former. This is confirmed by the computed Mulliken electronic charge transferred from the molecule to the gold tips of the nanobridges, q, which is reported also in Table 1. The increase of q with the molecular length runs parallel to the corresponding decrease of I, as confirmed by the values listed in Table 1. It is evident that the correctness of our predictions depends crucially on the accuracy of the computational method to correctly reproduce E_g. Recent KSDFT-B3LYP calculations on oligoacene molecules[88] indicate that they are rather accurate indeed, which makes us reasonably confident on the above conclusions.

In summary, the decrease of both I and E_g of the (circum)-acene molecules as their size increases favors the HOMO-E_F alignment, incrementing the conductance at zero bias, which explains the ordering found for $\mathscr{G}(E_F)$ in Figure 5 and summarized in point 1 above. On the other hand, the nonlinear growth of $\mathscr{G}(E_F)$ with the size of the molecule for the *ss* single-molecule as compared to the quite linear one observed for the corresponding *os* structures results from a combination of two facts: the Lorentzian form of the peak, on one side, and the Fermi level being positioned much more deeply in the molecular gap for the former type of structures, on the other. This explains

(97) Perdew, J. P.; Parr, R. G.; Levy, M.; Balduz, J. L., Jr. *Phys. Rev. Lett.* **1982**, *49*, 1691–1694.
(98) Levy, M.; Perdew, J. P.; Sahni, V. *Phys. Rev. A* **1984**, *30*, 2745–2748.

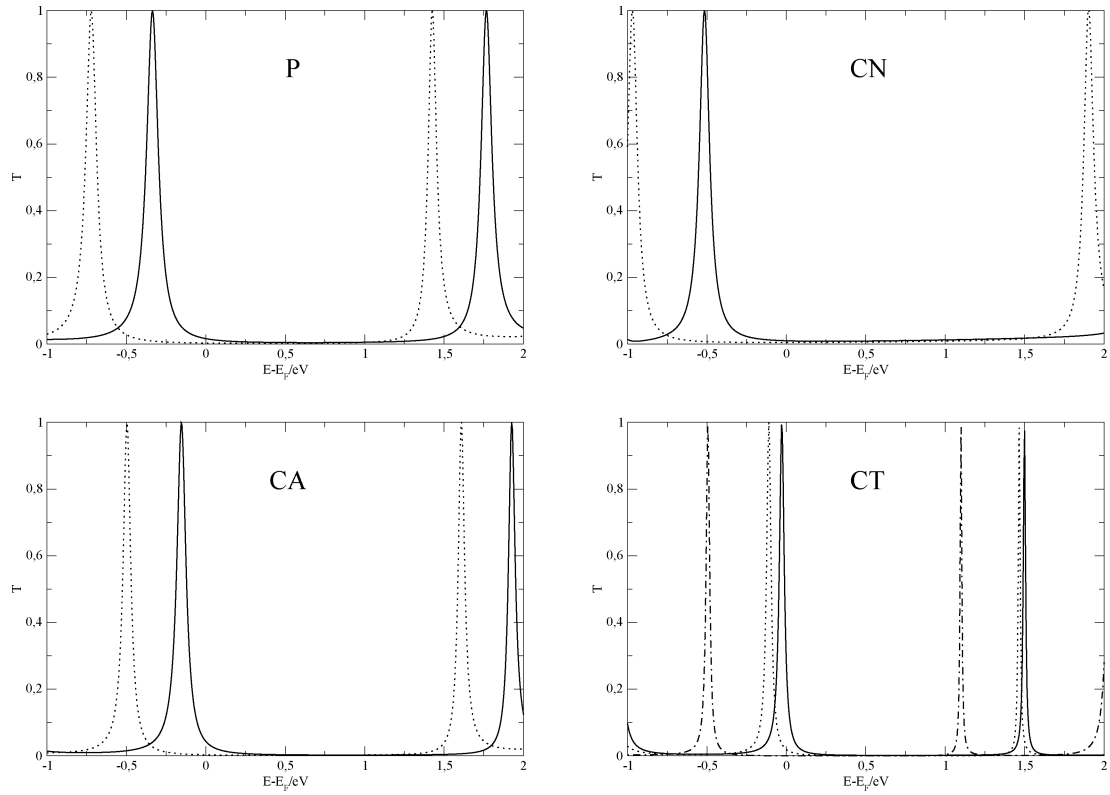

Figure 7. Transmission profiles of single-molecule *ss* gold−(circum)acene−gold nanobridges with varying charges. Solid, $Q = 0$; dotted, $Q = -0.5$; dot-dashed, $Q = -1.0$.

the remarkable conductance of about $0.2G_0$ calculated for the *ss* gold−CT−gold nanobridge.

The above findings further suggest that gold−CT−gold nanojunctions can be used to build efficient FETs, because increasing the electron charge of the nanojunction will displace the Fermi level toward the gap, resulting in a drastic lowering of the conductance as we move down along the resonance tail. Actually, this is confirmed by the reduction of almost an order of magnitude in $\mathscr{G}(E_F)$ when the negative charge is increased by 0.5e in *ss* structures (a similar trend is also observed in the *os* ones, but it is not reported for brevity): from $\sim 2 \times 10^{-2} G_0$ to $\sim 3 \times 10^{-3} G_0$ for P, from $\sim 1 \times 10^{-2} G_0$ to $\sim 5 \times 10^{-3} G_0$ for CA, from $\sim 4 \times 10^{-2} G_0$ to $\sim 3 \times 10^{-3} G_0$ for CN, and from $\sim 3 \times 10^{-1} G_0$ to $\sim 2 \times 10^{-2} G_0$ for CT. Further increase of the negative charge in P, CA, and CN *ss* nanobridges does not lead to further reductions in $\mathscr{G}(E_F)$, because the lowest transmission values in the gap have already been reached, as deduced from the evolution of the transmission profiles upon charging the system plotted in Figure 7. However, this is not the case for *ss* gold−CT−gold nanobridges, where increasing the negative charge to 1.0e further reduces $\mathscr{G}(E_F)$ about 3 orders of magnitude, from $\sim 3 \times 10^{-1} G_0$ to $\sim 4 \times 10^{-4} G_0$, pointing at these kind of nanobridges as potential candidates to build field effect transistors.

It is also evident that the proximity between the two tip apexes in single-molecule *os* nanobridges contributes significantly to the conductance, as shown by the comparatively large transmission in the molecular HOMO−LUMO gap region. The interaction between the frontier molecular states and the metallic tips is also different in both kind of structures (*os* vs *ss* ones), which translates into reduced HOMO−LUMO-derived resonance gaps, Δ_g, in the former; compare the top-left with the top-right panel of Figure 6, and the corresponding data in Table 1. This is also in agreement with recent theoretical calculations, suggesting that the Au−C bond is strengthened when two gold atoms bind to nearby carbons in a pentacene molecule.[77] The combined result of these two effects is a conductance at zero bias of almost an order of magnitude lower for most of the single-molecule *ss* nanojunctions compared to that calculated for the single-molecule *os* ones, as already mentioned in point 2 above.

3.2. Nanojunctions with Several π-Stacked Molecules. Unfortunately, complete control on the fabrication process of a nanodevice might be difficult to achieve,[90,91] and thus it is not unlikely that not only one but several molecules could bridge the gap between the metallic leads. In fact, it has been observed experimentally that molecular π-stacking is not uncommon in the fabrication of graphene-based nanojunctions.[14,28] With this features in mind we will address now the effect of molecular π stacking on the conductance of gold−(circum)acene−gold nanobridges. As already commented in section 2.2 we will consider two extreme cases: perfectly cofacial stacks and parallel-displaced stacks. The former are optimal with respect to the overlap while the latter are energetically favored.

3.2.1. Cofacially π-Stacked Molecules. We first want to note that the differences between the conductance of *os* and *ss* structures observed in the previous section for single-molecule nanojunctions are much less pronounced for cofacially π-stacked two-molecule nanobridges (see Figure 5), as it should be expected, because the metallic tips are now quite far apart from each other in the *os* nanobridges (see Figures 2 and 3). Thus, the "direct" tip−tip contribution to $\mathscr{G}(E_F)$ and the particular interaction between the tips and the molecular frontier orbitals characteristic of single-molecule *os* nanobridges are now absent in the two-molecule ones. On the other hand, a new ingredient must be considered in π-stacked nanobridges: the progressive lowering of I and E_g as the number of molecules in the stack

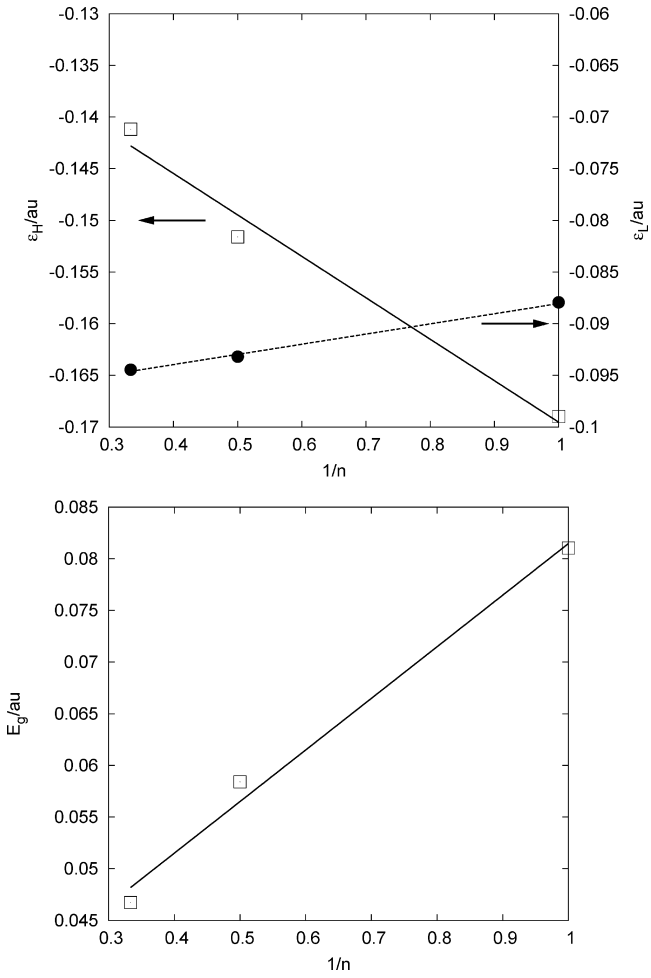

Figure 8. Top: Evolution of ε_H (squares; left axis) and ε_L (circles; right axis) with the inverse of the number of π-stacked molecules (n) in *ss* gold-pentacene-gold nanobridges. Bottom: Evolution of the corresponding HOMO−LUMO gap for the same systems. The lines represent the corresponding linear fits to the data.

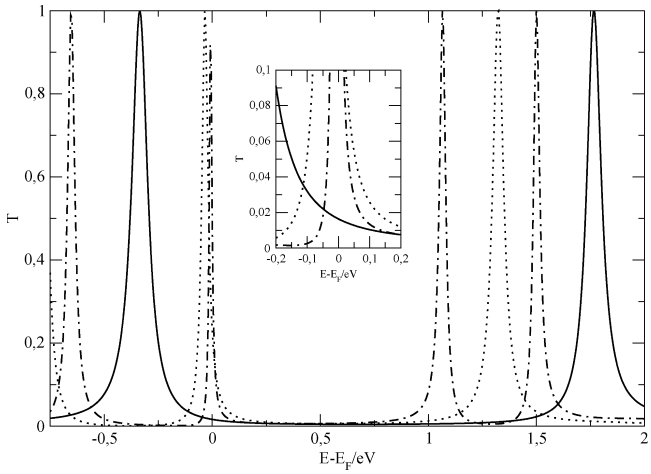

Figure 9. Transmission profiles of single-molecule and cofacially-π-stacked *ss* gold−P−gold nanobridges near the Fermi level. Solid, × 1; dotted, × 2; dotted-dashed, × 3.

increases, which reflects in the corresponding destabilization (stabilization) of the ε_H (ε_L) of the isolated dimers with respect to the monomer, as Table 1 indicates. This brings the maximum of the corresponding resonance closer to the Fermi level, which

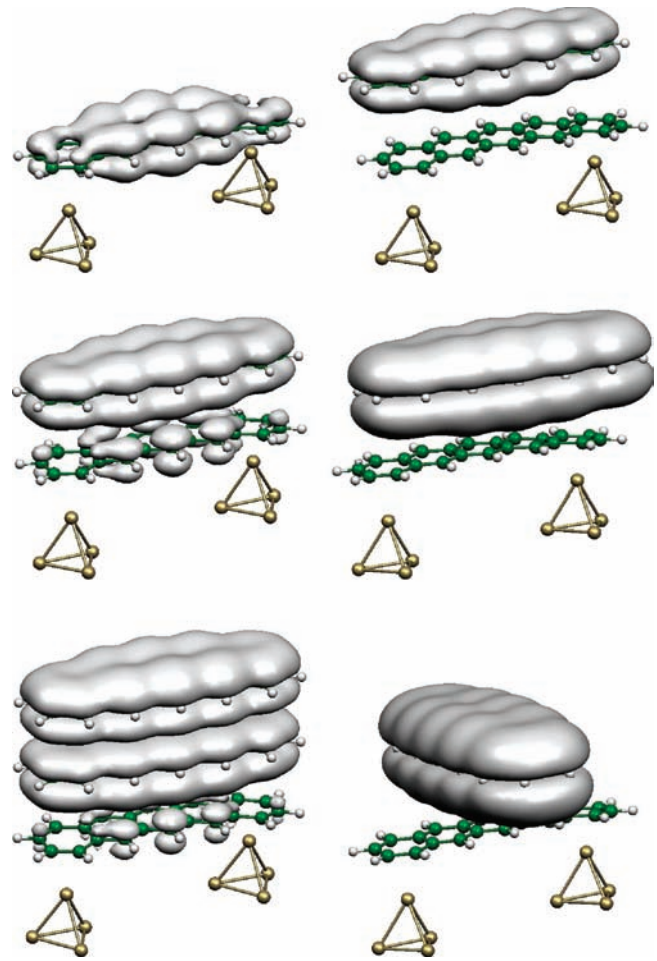

Figure 10. Contour plots of the HOMO-derived resonance of *ss* gold−P−gold nanobridges. Left: cofacial structures; from top to bottom, × 1, × 2, × 3. Right: noncofacial structures; from top to bottom, × 2-PD1, × 2-PD2, × 2-TS.

explains the tremendous increase in $\mathcal{T}(E_F)$ for the *ss* structures, which are now on the same order of magnitude than those corresponding to *os* ones for all the molecules considered. Both facts justify the findings summarized in point 3 at the beginning of section 3.

The pronounced variation in ε_H and ε_L, and the corresponding reduction of E_g, with the number of molecules present in the π stack, n, has been previously observed in π-stacked thiophene complexes,[99] with an almost linear dependence of ε_H, ε_L, and E_g with $1/n$. To check if this is also the case for (circum)acenes we have performed additional calculations increasing the number of molecules in the π stack that bridge the *ss* structures. We focus on this kind of nanobridges to find out how much their comparatively low single-molecule conductance can increase by adding molecules to the stack. On the other hand, we have only considered pentacene for this kind of study because it is the smallest of the three molecules considered, thus making the corresponding computational problem affordable. Figure 8 plots ε_H, ε_L, and E_g as a function of $1/n$, with n being the number of pentacene molecules in the stack, and clearly shows the linear dependence found in ref 99. This trend is consistent with the increased alignment between the transmission peak associated with the HOMO-derived resonance and the Fermi level, as

(99) Rodríguez-Ropero, F.; Casanovas, J.; Alemán, C. *J. Comput. Chem.* **2007**, *29*, 69–78.

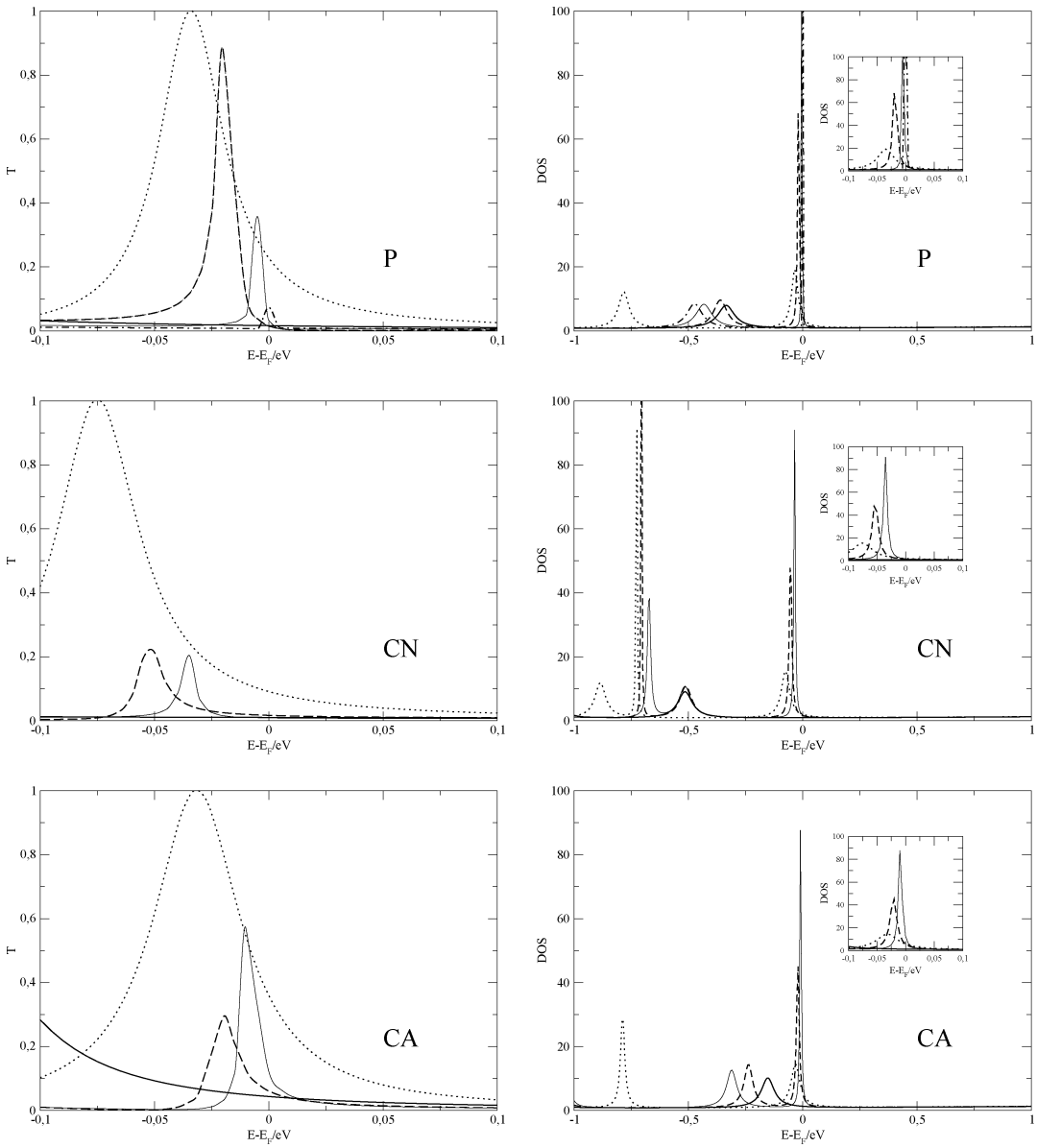

Figure 11. Transmission profiles (left) and density of states (right) near the Fermi level of gold−(circum)acene-−old *ss* structures. Dark solid, *ss* × 1; dotted, *ss* × 2 cofacial; light solid, *ss* × 2-PD1; dashed, *ss* × 2-PD2; dotted-dashed, *ss* × 2-TS.

reflected in Figure 9, which explains the increase in conductance with the number of molecules present in the π stack, as already shown in Figure 5 and indicated in point 4 above. In agreement with reduced I and E_g values, such alignment is also favored by larger charge transfers from the molecular arrangement to the gold tips as the number of molecules in the stack increases; see Table 1. Thus, the π-stacking of (circum)acenes and similar graphene-based molecules should be taken into account when fabricating nanodevices based on this kind of molecules, because it represents an appealing way to alter their conductance properties through the corresponding modification of the band-gap and ionization potential of the molecular arrangement. The trends reported in Figures 5 and 8 and Table 1 suggest that quite high conductances could be achieved if a sufficient number of molecules is present in the stack.

However, we also want to point out the decrease in the peak width as the number of molecules in the stack increases. This is a consequence of a lower molecule-metal overlap caused by the redistribution of the orbital density over the increasing volume of the molecular region, as reflected by the contour plots of the HOMO-derived resonance peak shown in Figure 10. Indeed, the overlap loss caused by noncofacial π-stackings strongly affects the conductance of the nanodevice, as will be highlighted in the next section.

3.2.2. Non-Cofacially π-Stacked Molecules. The amount of π overlap in the stack diminishes also as the perfect cofacial arrangement between the molecules is lost as the electronic cloud concentrates in the upper molecule, as evidenced by the contour plots of the HOMO-derived resonances corresponding to the *ss* × 2-TS, *ss* × 2-PD1, and *ss* × 2-PD2 gold−P−gold structures shown in Figure 10, leading to a strong reduction of $\mathscr{T}(E_F)$ caused by the corresponding reduction of the peak width shown in Figure 11, where the transmission profiles have been plotted.

The shrinking of the peak is specially dramatic for the pentacene *ss* × 2-PD1 structure, because the two molecules are displaced by an amount that is almost equal to their width. For the two circumacene molecules the PD1 and PD2 structures

are of a similar width, thanks to the additional "row" of fused benzene rings. On the other hand, the relative trends observed for their cofacial partners are also kept in the displaced structures, because the relative ordering of the ionization potentials and gaps found in the former are also observed in the latter, as can be checked in Table 1. Certainly, the HOMO resonances are much closer to the Fermi level for the displaced structures than for the cofacial ones, despite the former having higher I and Δ_g values than the latter; but this is also a consequence of the reduced width of the corresponding density-of-states (DOS) peaks, which are also shown in Figure 11. Summing up, the value of $\mathscr{G}(E_F)$ for the *ss* × 2-PD1 CA structure doubles the single-molecule one; a result that is also expected for CT, as suggested by the values of I and E_g for the PD1 and PD2 CT isolated dimers reported in Table 1. Thus, the conductance enhancement observed for the cofacial dimers is also found in the parallel-displaced ones, but to a modest extent, a fact that should not be overlooked for this kind of systems.

4. Summary and Conclusions

We can sum up the above analysis by interpreting the findings of the previous section in the following way: the low bias conductance of gold−(circum)acene−gold molecular nanobridges depends on the line up between the Fermi level and a HOMO-derived resonance, which is favored by:

1. The proximity of the metallic tips when they are placed at each side of the molecular plane, allowing for a direct metal−metal contribution and energy shifts of the molecular states.

2. The length of the molecule: larger lengths lead to lower ionization potentials and gaps, and higher charge transfers between the molecule and the gold leads.

3. The number of molecules present in a π stack: the larger this number, the lower the ionization potential, the gaps, and the amount of overlap between molecular and metallic states, and the larger the charge transferred from the molecules to the gold leads.

4. A perfect cofacial π-stacked arrangement: favoring the overlap between the molecular arrangement and the metallic tips.

Although we are fully aware of the limitations affecting state-of-the-art conductance calculations as regards the absolute values of $\mathscr{G}$, they are much more reliable to ascertain relative trends. The ones listed above suggest that gold-circumacene-gold nanobridges could be used as versatile nanodevices for molecular electronics, given their conductance-length relationship, with circumtetracene providing the highest conductance on a variety of molecule-tip arrangements. Large "on" conductances and on−off ratios for FETs fabricated with these nanojunctions are also expected, whereas contingent π-stacking growth can increase or reduce the conductance, depending on this taking place cofacially or not. We believe that these findings are useful to better understand and design the conductance properties of molecular nanojunctions based on graphene-related materials, such as those analyzed here.

Acknowledgment. Financial support from Spanish Ministerio de Educación y Ciencia (MEC) and the European Regional Development Fund through Project CTQ2007-66461/BQU. J.C.S.G. thanks the Spanish MEC and the Generalitat Valenciana for economic support within the "Ramón y Cajal" program.

Supporting Information Available: Complete ref 84. This material is available free of charge via the Internet at http://pubs.acs.org.

JA904372D